

## Caloric curve for finite nuclei in relativistic models

*D.P.Menezes*<sup>1</sup> and *C. Providência*<sup>2</sup>

<sup>1</sup> *Depto de Física - CFM - Universidade Federal de Santa Catarina  
Florianópolis - SC - CP. 476 - CEP 88.040 - 900 - Brazil*

<sup>2</sup> *Centro de Física Teórica - Depto de Física - Universidade de Coimbra  
3004-516, Coimbra - Portugal*

### Abstract

In this work we calculate the caloric curve (excitation energy per particle as a function of temperature) for finite nuclei within the non-linear Walecka model for different proton fractions. It is shown that the caloric curve is sensitive to the proton fraction. Freeze-out volume effects in the caloric curve are also studied.

PACS number(s): **21.10.-k, 21.30.-x, 21.65.+f, 25.70.-z**

The production of several intermediate mass fragments in a short time scale during heavy ion collisions is known as nuclear multifragmentation. At several hundred MeV/u, the multifragment decay follows the formation of an equilibrated projectile remnant. The existence of equilibration is consistent with different experimental observations, such as the symmetry of the measured rapidity distributions of fragments with  $Z \geq 3$  [1]. The spectator matter has, therefore, been used to investigate a thermally driven liquid-gas phase transition [1, 2, 3]. One of the evidences of this transition in infinite systems is the fact that the heat-capacity exhibits a peak at a given temperature. However in finite systems the situation is more complicated [2, 4, 5, 6]. The caloric equation of state, which is given by the excitation energy per nucleon in terms of the thermodynamic temperature is an important quantity to be investigated in the search for a signal of a phase transition. Nevertheless, it was recently pointed out that the identification of the existence of a phase transition cannot be based only on the behaviour of the caloric curve and a more detailed knowledge of the thermodynamic phase diagram is also required [7]. In particular it was shown that the interpretation of the data is sensitive to the use of a variable free volume on the calculation.

Recently there has been a big development in the description of nuclei and nuclear matter in terms of relativistic many-body theory. In particular, the phenomenological models developed using the relativistic mean-field theory describe well the ground-state of both stable and unstable nuclei [8, 9]. These same models are used to describe the properties of neutron stars and super-novae [10]. Therefore, it is important to test these models at finite temperature and different densities. In particular, it would be interesting to compare the caloric curve obtained within a relativistic Thomas-Fermi calculation with the recent experimental data, and verify whether the proton-neutron asymmetry of the hot source gives information on the symmetry energy term of these models.

Within the framework of relativistic models, the liquid-gas phase transition in nuclear matter has been investigated at zero and finite temperatures for symmetric and asymmetric semi-infinite systems [10, 11, 12, 13, 14]. With the help of the Thomas Fermi approximation, we have investigated droplet formation in the liquid-gas phase transition in cold [15, 16] and hot [17] asymmetric nuclear matters using the non-linear Walecka model (NLWM) [8, 18]. As shown in Refs. [15, 17], the optimal nuclear size of a droplet in a neutron gas is determined by a delicate balance between nuclear Coulomb and surface energies. The surface energy favors nuclei with a large number of nucleons  $A$ , while the nuclear Coulomb self-energy favors small nuclei.

In the present work we calculate the caloric curve, given by the temperature dependent excitation energy per particle, for the nuclei obtained with the approach mentioned above. In particular, we will study the influence of the proton-neutron asymmetry. We chose the systems  $^{150}\text{Sm}$  and  $^{166}\text{Sm}$  because they lie in the mass and charge range of interest for the experiments we are analysing [1, 2, 21]. In the first two references the caloric curve presented is obtained with prefragments in the mass range  $50 \sim 100$  to  $200$ . In the third reference the data were obtained for a compound nucleus of mass  $\sim 160$ . We took two isotopes with quite different number of neutrons in order to study the effect of proton-neutron asymmetry. In the framework of the Thomas-Fermi theory, shell effects are washed out. Hence, we are calculating average properties. We expect that the caloric curve of a given system may depend quantitatively on the system mass but the qualitative features, namely the dependence of proton-neutron asymmetry and the effect of freeze-out volume, will be similar. In multifragmentation calculations an input parameter called the freeze-out radius is normally used [4], so that a phase transition at constant volume is simulated. We investigate the consequences on the caloric curve when thermalization in

a freeze-out volume is imposed in the present framework.

We start from the Lagrangian density of the relativistic non-linear Walecka model [18], [19]

$$\begin{aligned} \mathcal{L} = & \bar{\psi} \left[ \gamma_\mu \left( i\partial^\mu - g_v V^\mu - \frac{g_\rho}{2} \vec{\tau} \cdot \vec{b}^\mu - eA^\mu \frac{(1 + \tau_3)}{2} \right) - (M - g_s \phi) \right] \psi \\ & + \frac{1}{2} (\partial_\mu \phi \partial^\mu \phi - m_s^2 \phi^2) - \frac{1}{3!} \kappa \phi^3 - \frac{1}{4!} \lambda \phi^4 - \frac{1}{4} \Omega_{\mu\nu} \Omega^{\mu\nu} + \frac{1}{2} m_v^2 V_\mu V^\mu \\ & - \frac{1}{4} \vec{B}_{\mu\nu} \cdot \vec{B}^{\mu\nu} + \frac{1}{2} m_\rho^2 \vec{b}_\mu \cdot \vec{b}^\mu - \frac{1}{4} F_{\mu\nu} F^{\mu\nu}, \end{aligned} \quad (1)$$

where  $\phi$ ,  $V^\mu$ ,  $\vec{b}^\mu$  and  $A^\mu$  are, respectively, the scalar-isoscalar, vector-isoscalar, vector-isovector meson fields and the electromagnetic field;  $\Omega_{\mu\nu} = \partial_\mu V_\nu - \partial_\nu V_\mu$ ,  $\vec{B}_{\mu\nu} = \partial_\mu \vec{b}_\nu - \partial_\nu \vec{b}_\mu - g_\rho (\vec{b}_\mu \times \vec{b}_\nu)$  and  $F_{\mu\nu} = \partial_\mu A_\nu - \partial_\nu A_\mu$ , with the following parameters: the nucleon mass  $M = 938$  MeV, the masses of the mesons  $m_s = 492.25$  MeV,  $m_v = 795.36$  MeV,  $m_\rho = 763.0$  MeV, the electromagnetic coupling constant  $e = \sqrt{\frac{4\pi}{137}}$  and the self-interacting coupling constants  $\kappa$  and  $\lambda$ . The set of constants we use is normally identified as NL1 [8], with  $C_i^2 = g_i^2 M^2 / m_i^2$ ,  $i = s, v, \rho$ , where  $C_s^2 = 373.176$ ,  $C_v^2 = 245.458$ ,  $C_\rho^2 = 149.67$ ,  $\kappa/M \times 10^{-3} = 2g_s^3 \times 2.4578$  and  $\lambda \times 10^{-3} = -6g_s^4 \times 3.4334$ . This parameterization gives a good description of the ground-state properties of all stable nuclei.

The thermodynamic potential is obtained within the Thomas–Fermi approximation. After it is minimized in terms of the meson and electromagnetic fields, the following coupled differential equations have to be solved:

$$\nabla^2 \phi = m_s^2 \phi + \frac{1}{2} \kappa \phi^2 + \frac{1}{3!} \lambda \phi^3 - g_s \rho_s, \quad (2)$$

$$\nabla^2 V_0 = m_v^2 V_0 - g_v \rho_B, \quad (3)$$

$$\nabla^2 b_0 = m_\rho^2 b_0 - \frac{g_\rho}{2} \rho_3, \quad (4)$$

$$\nabla^2 A_0 = -e \rho_p, \quad (5)$$

where

$$\rho_s = 2 \sum_{i=p,n} \int \frac{d^3 p}{(2\pi)^3} \frac{M^*}{\epsilon} (f_{i+} + f_{i-}),$$

with

$$f_{i\pm}(\mathbf{r}, \mathbf{p}, t) = \frac{1}{1 + \exp[(\epsilon \mp \nu_i)/T]}, \quad i = p, n, \quad (6)$$

where  $\nu_i = \mu_i - \mathcal{V}_{i0}$  are the effective chemical potentials with  $\mu_i$  being the chemical potentials for particles of type  $i$  and

$$\mathcal{V}_{p0} = g_v V_0 + \frac{g_\rho}{2} b_0 + e A_0, \quad \mathcal{V}_{n0} = g_v V_0 - \frac{g_\rho}{2} b_0;$$

$\epsilon = \sqrt{p^2 + M^{*2}}$ ,  $M^* = M - g_s \phi$  is the effective nucleon mass and  $T$  is the temperature. Moreover,  $\rho_B = \rho_p + \rho_n$ ,  $\rho_3 = \rho_p - \rho_n$  with

$$\rho_i = 2 \int \frac{d^3 p}{(2\pi)^3} (f_{i+} - f_{i-}), \quad i = p, n, \quad (7)$$

and the energy density, obtained from the thermodynamic potential reads:

$$\begin{aligned} \mathcal{E}(r) = & 2 \sum_i \int \frac{d^3 p}{(2\pi)^3} [\epsilon(f_{i+} + f_{i-}) + \mathcal{V}_{i0}(f_{i+} - f_{i-})] \\ & + \frac{1}{2} [(\nabla\phi)^2 - (\nabla V_0)^2 - (\nabla b_0)^2 - (\nabla A_0)^2] \\ & + \frac{1}{2} \left( m_s^2 \phi^2 + \frac{2}{3!} \kappa \phi^3 + \frac{2}{4!} \lambda \phi^4 - m_v^2 V_0^2 - m_\rho^2 b_0^2 \right). \end{aligned} \quad (8)$$

The coupled differential equations are solved numerically. For more details on the analytical and numerical procedure, please refer to [15, 17]. Three kinds of instabilities can occur in this system. The condition for mechanical stability requires that  $\left(\frac{\partial P}{\partial \rho_B}\right)_{Y_p} \geq 0$ , where  $P$  is the pressure and  $Y_p = \rho_p/\rho_B$  is the proton fraction. The condition for diffusive stability implies the inequalities  $\left(\frac{\partial \mu_p}{\partial Y_p}\right)_{P,T} \geq 0$  and  $\left(\frac{\partial \mu_n}{\partial Y_p}\right)_{P,T} \leq 0$ . Finally, the thermodynamical stability is expressed by  $C_v = \left(\frac{d\varepsilon^*}{dT}\right)_{v,Y_p} > 0$ , where  $C_v$  is the specific heat and  $\varepsilon^* = \varepsilon(T) - \varepsilon(T=0)$  is the excitation energy per particle, with the total energy per particle at any temperature given by [20]  $\varepsilon(T) = \int \frac{\mathcal{E}(r)}{A} d^3 r$ , where  $A = Z + N$ . The two-phase liquid-gas coexistence is governed by the Gibbs condition.

We have first solved the equations of motion for an infinite system in order to obtain appropriate boundary conditions for the program which integrates the set of coupled non-linear differential equations (2) to (5) in the Thomas-Fermi approximation. Once the fields are obtained, all thermodynamic quantities of interest can be easily calculated. The binding energy per nucleon is  $\frac{B}{A} = \varepsilon(T) - 938$ . MeV.

In table 1, we show the binding energy per nucleon and the excitation energy per particle for the  $^{150}_{62}\text{Sm}_{88}$ , which has a proton fraction equal to 0.41. In table 2, the same quantities are shown for the  $^{166}_{62}\text{Sm}_{104}$ , with a proton fraction of 0.37. Notice that, independently of the proton fraction, the excitation energy per particle increases with temperature in the range of temperatures shown. For higher temperatures we were not able to obtain convergence for a droplet of the size considered.

In tables 3 and 4, we give the binding and the excitation energies per particle when a freeze-out volume of respectively  $6V_0$  and  $9V_0$  is used with  $V_0$  the volume at  $T = 0$ . We have considered a freeze-out radius of  $2.2A^{1/3}$  fm for  $6V_0$  and  $2.5A^{1/3}$  fm for  $9V_0$  with  $A = 166$ . In this case the solutions obtained consist of a droplet immersed in a gas of evaporated particles, in such a way that they mimic a source of changing mass. As temperature increases more particles evaporate, mainly neutrons, and the fraction of protons in the droplet increases. This can be seen in tables 3 and 4 where the number of particles which remain inside the droplet as well as the droplet proton fraction ( $Y_d$ ) are given. We conclude that the larger the freeze-out volume the faster the excitation energy increases with temperature and the larger is the proton fraction in the droplet. This picture is consistent with the discussion presented in [6].

The results for the excitation energies shown in all tables are displayed in figure 1. Also shown are the experimental data of refs. [1, 2], and the Fermi-gas law  $\varepsilon^* = 1/kT^2$ , with  $k = 10.0$  (thin dashed line) and  $13.0$  (thin full line). We have considered that the measured temperature  $T_{\text{HeLi}}$  ( $T_{\text{HeTD}}$ ), obtained from the isotope yield ratios  $^3\text{He}/^4\text{He}$  and  $^6\text{Li}/^7\text{Li}$  ( $^3\text{He}/^4\text{He}$  and  $^2\text{H}/^3\text{H}$ ), satisfy, in the range of densities considered,  $T_{\text{exp}}/T \sim 0.85$  and have scaled the experimental data accordingly [2].

We conclude that the excitation energy for  $^{166}\text{Sm}$  (thick long-dashed curve), proton fraction 0.37, increases slightly slower with temperature than for  $^{150}\text{Sm}$  (thick full curve), proton fraction 0.41, although the difference is not large. These two curves are consistent with data of [21] and a level density parameter  $A/k$ ,  $k = 13.0$  in the Fermi gas model relation. This agrees with the observed value at around 2 MeV excitation energies [21]. Experimental results obtained at higher bombarding energies [1, 2] give higher excitation energies for the same temperatures. It can be seen from figure 1 of ref. [2] that the higher excitation energies correspond to smaller sources. The larger sources with an average  $Z_{\text{bound}} \geq 60$  have excitation energies  $\varepsilon^* \leq 5$  MeV. In the present approach the solutions obtained in a fixed volume, correspond to droplets in a gas of free particles.

These solutions have higher excitation energies than the ones obtained with no *a priori* fixed volume. In average, this situation corresponds to smaller systems at higher energies. This could explain the change of slope that is observed in the calculated data both for  $V = 6 V_0$  and  $V = 9 V_0$ , in such a way that they come closer to the experimental data [1, 2]. The same effect was obtained in ref. [23], where an exact analytical solution of the statistical multifragmentation model was found in the thermodynamic limit. For a fixed nucleon density, the caloric curve rises more slowly for lower densities and its leveling occurs at lower temperatures. The leveling of the caloric curve is associated with the fast change of the configurations from a state dominated by one liquid fragment to a gaseous multifragment configuration. We can draw a similar conclusion from tables 3, 4 and figure 1: the leveling of the thick dash-dotted and short-dashed curves occurs faster when the droplet (liquid phase) becomes smaller. It would be interesting to study the effect of the symmetry energy on the leveling of the caloric curve in the statistical multifragmentation model of ref. [23].

In summary, we have studied the excitation energies of arising droplets in a vapor system, up to  $T = 6.5$  MeV. The droplets are described in terms of a non-linear Walecka-type model within the Thomas-Fermi approximation. We have used the NL1 parameterization, which is known to describe well the ground-state properties of nuclei. The excitation energies of droplets either corresponding to  $^{150}\text{Sm}$  or  $^{166}\text{Sm}$ , for temperatures between 3 and 6.5 MeV, are consistent with the caloric curve in the Fermi gas approximation with a level density parameter  $A/13$ . This result agrees with experimental data obtained in heavy-ion collisions at intermediate energies [21]. We have shown that the caloric curve is sensitive to the proton fraction and therefore to the symmetry term of the model used. Experimentally the dependence on the proton fraction could be studied by comparing data obtained from sources with different proton fractions. For the range of temperatures studied, the NL1 parameterization of the non-linear Walecka model has shown to be adequate to describe nuclear properties and therefore it is a good candidate to generate an equation of state for astrophysical purposes.

When a freeze-out radius is imposed, our procedure yields caloric curves which come closer to the experimental results obtained in heavy-ion collisions at higher energies [1, 2]. In this case we have smaller droplets with a higher proton fraction immersed in a gas of particles, mainly neutrons. This could be interpreted as an oversimplified picture of the second regime in the statistical model prediction [22], namely the coexistence phase with

a multifragment mixture. This interpretation is supported by the results of ref. [23].

Although the thermodynamical equilibrium analysis oversimplifies the problem of high energy heavy-ion collisions it is useful for providing a concrete description of warm nuclei and for showing qualitative features that should be present in more microscopic calculations.

### Acknowledgments

We acknowledge the computation facilities offered by Centro de Física Computacional of the University of Coimbra. C. P. would also like to thank the warm hospitality in the Departamento de Física, Universidade Federal de Santa Catarina. This work was partially supported by CNPq - Brazil and CFT - Portugal under the contracts PRAXIS/2/2.1/FIS/451/94 and POCTI/1999/FIS/35308.

### References

- [1] J. A. Hauger *et al.*, Phys. Rev. Lett. **77**,235 (1996).
- [2] J. Phochodzalla *et al.*, Phys. Rev. Lett. **75**, 1040 (1995).
- [3] Y. G. Ma *et al.*, Phys. Lett. **B 390**,41 (1997).
- [4] A. Chbihi, O. Schapiro, D.H.E. Gross and S. Salou, Eur. Phys. J. **A5**,251 (1999).
- [5] J.D. Frankland *et al.*, Nucl. Phys. in press, npa5852.
- [6] A.B. Larionov, A.S. Botvina, M. Colonna, M. Di Toro, Nucl. Phys. **A658**, 375 (1999).
- [7] J. B. Elliott and A. S. Hirsch, Phys. Rev C **61**, 054605 (2000).
- [8] P.-G. Reinhard, M. Rufa, J. Maruhn, W. Greiner and J. Friedrich, Z. Phys. **A 323**,13 (1986).
- [9] Y. Sugahara and H. Toki, Nucl. Phys. **A579**,557 (1994).
- [10] H. Schen, H. Toki, K. Oyamatsu and K. Sumiyoshi, Nucl. Phys. **A637**,435 (1998);  
K. Sumiyoshi and H. Toki, Ap. J. **422**,700 (1994).

- [11] H. Reinhardt and H. Schulz, Nucl. Phys. **A432**,630 (1985).
- [12] H. Müller and R.M. Dreizler, Nucl. Phys. **A563**,649 (1993).
- [13] D. Von Eiff, J. M. Pearson, W. Stocker and M. K.Weigel, Phys. Lett. **B324**,279 (1994).
- [14] M. Centelles, M. Del Estal and X. Viñas, Nucl. Phys. **A635**,193 (1998).
- [15] D.P. Menezes and C. Providência, Nucl. Phys. **A650**, 283 (1999).
- [16] G. Krein, D. Menezes, M. Nielsen and C. Providência, Nucl. Phys. **A674**,125 (2000).
- [17] D.P. Menezes and C. Providência, Phys. Rev. C **60**, 024313 (1999).
- [18] J. Boguta and A. R. Bodmer, Nucl. Phys. **A292**,413 (1977); A.R. Bodmer and C.E. Price, Nucl. Phys. **A505**,123 (1989); A.R. Bodmer, Nucl. Phys. **A526**,703 (1991).
- [19] Y.K. Gambir, P. Ring, A. Thimet, Ann. Phys. **198**,132 (1990); H. Berghammer, D. Vretenar and P. Ring, Phys. Lett. **B296**,290 (1992); D. Vretenar, H. Berghammer and P. Ring, Phys. Lett. **B319**,29 (1993); H. Berghammer, D. Vretenar and P. Ring, Nucl. Phys. **A560**,1014 (1993).
- [20] J. N. De, S. Gupta, S. Shlomo and S. K. Samaddar, Phys. Rev C **55**,R1641 (1997).
- [21] K. Hagel et *al.*, Nucl. Phys. **A486**,429 (1988).
- [22] J. P. Bondorf, A. S. Botvina, A. S. Iljinov, I. N. Mishustin and K. Sneppen, Phys. Rep. **257**,133 (1995).
- [23] K. A. Bugaev, M. I. Gorenstein, I. N. Mishustin and W. Greiner, nucl-th/0011055; K. A. Bugaev, M. I. Gorenstein, I. N. Mishustin and W. Greiner, Phys. Rev C **62**, 044320 (2000).



**Table 1.** Output results given by the solution of the coupled differential equations for different temperatures for  $^{150}_{62}\text{Sm}_{88}$  ( $Y_p = 0.41$ ).

$T$	$B/A$	$\varepsilon^*(T)$
(MeV)	(MeV/A)	(MeV/A)
0.	-8.2	0.0
3.	-7.6	0.7
4.	-7.1	1.2
5.	-6.4	1.8
6.	-5.4	2.8
6.5	-4.8	3.4

**Table 2.** Output results given by the solution of the coupled differential equations for different temperatures for  $^{166}_{62}\text{Sm}_{104}$  ( $Y_p = 0.37$ ).

$T$	$B/A$	$\varepsilon^*(T)$
(MeV)	(MeV/A)	(MeV/A)
0	-7.9	0.0
2.	-7.7	0.3
2.5	-7.5	0.4
3.	-7.3	0.7
4.	-6.8	1.1
5.	-6.1	1.8
6.	-5.2	2.7
6.5	-4.8	3.1

**Table 3.** Output results given by the solution of the coupled differential equations for different temperatures for  ${}^{166}_{62}\text{Sm}_{104}$  in a fixed volume,  $6V_0$ .

$T$ (MeV)	$B/A$ (MeV/A)	$\varepsilon^*(T)$ (MeV/A)	$A$	$Y_d$
0.	-7.9	0.0	166	0.37
3.	-7.1	0.8	163	0.38
4.	-6.3	1.6	158	0.39
5.	-5.4	2.5	154	0.40
6.	-3.9	4.0	148	0.40
6.5	-3.0	4.9	143	0.40

**Table 4.** The same as figure 3 for a fixed volume,  $9V_0$ .

$T$ (MeV)	$B/A$ (MeV/A)	$\varepsilon^*(T)$ (MeV/A)	$A$	$Y_d$
0.	-7.9	0.0	166	0.37
3.	-7.0	0.9	161	0.38
4.	-6.2	1.7	156	0.39
5.	-5.1	2.8	150	0.41
6.	-3.4	4.5	142	0.41
6.5	-2.2	5.3	134	0.41

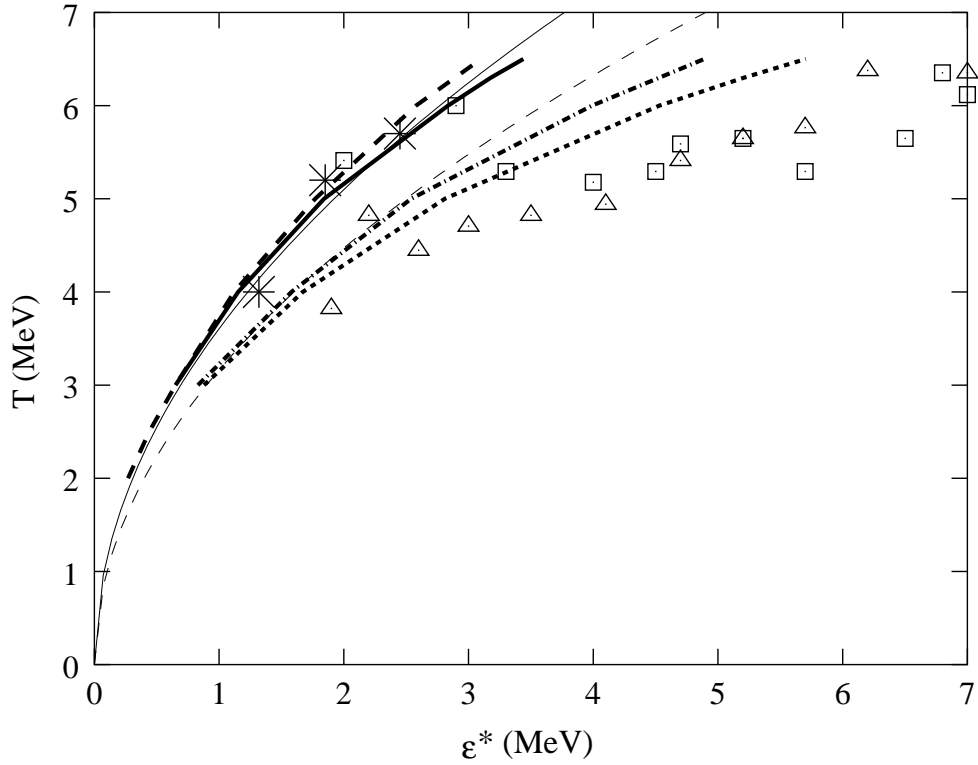


Figure 1: The caloric curves are shown for  $^{166}_{62}\text{Sm}_{104}$  ( $Y_p = 0.37$  - thick long-dashed line),  $^{150}_{62}\text{Sm}_{88}$  ( $Y_p = 0.41$  - thick full line); at  $6V_0$  (thick dash-dotted line) and  $9V_0$  (thick short-dashed line) fixed volumes for  $^{166}\text{Sm}$ , and for the Fermi gas law [21] ( $k = 10.0$  - thin dashed line and  $k = 13.0$  - thin full line). Experimental results from [2] (squares), [1] (triangles) and [21] (big stars) are also displayed.